Title

Wide-gap layered oxychalcogenide semiconductors: materials, electronic structures and optoelectronic properties.

Authors

Kazushige Ueda [1, 2], Hidenori Hiramatsu [2], Masahiro Hirano [2], Toshio Kamiya [2, 3] and Hideo Hosono [2, 3, 4]

Affiliations

[1] Department of Materials Science, Faculty of Engineering, Kyushu Institute of Technology, 1-1 Sensui-cho, Tobata-ku, Kitakyushu 804-8550, JAPAN

[2] Exploratory Research for Advanced Technology – Solution-Orientated Research for Science and Technology (ERATO – SORST), Japan Science and Technology Agency (JST), in the Frontier Collaborative Research Center (FCRC), S2-6F, Mail-box S2-13, Tokyo Institute of Technology, 4259 Nagatsuta-cho, Midori-ku, Yokohama 226-8503, JAPAN

[3] Materials and Structures Laboratory, Tokyo Institute of Technology, 4259 Nagatsuta-cho, Midori-ku, Yokohama 226-8503, JAPAN

[4] Frontier Collaborative Research Center (FCRC), Tokyo Institute of Technology, 4259 Nagatsuta-cho, Midori-ku, Yokohama 226-8503, JAPAN

Corresponding author

Kazushige Ueda (E-mail: kueda@che.kyutech.ac.jp,

Tel: +81-093-884-3339, Fax: +81-093-884-3300)

Keywords

Wide gap semiconductor, layered oxychalcogenide, electronic structure, photoemission spectroscopy, energy band calculation

Abstract

Applying the concept of materials design for transparent conductive oxides to layered oxychalcogenides, several *p*-type and *n*-type layered oxychalcogenides were proposed as wide-gap semiconductors and examined their basic optical and electrical properties. The layered oxychalcogenides are composed of ionic oxide layers and covalent chalcogenide layers, which bring wide-gap and conductive properties to these materials, respectively. The electronic structures of the materials were examined by normal/inverse photoemission spectroscopy and energy band calculations. The results of the examinations suggested that these materials possess unique features more than simple wide gap semiconductors. Namely, the layered oxychalcogenides are considered to be extremely thin quantum wells composed of the oxide and chalcogenide layers or 2D chalcogenide crystals/molecules embedded in an oxide matrix. Observation of step-like absorption edges, large band gap energy and large exciton binding energy demonstrated these features originating from 2D density of states and quantum size effects in these layered materials.

Introduction

Inorganic compounds are frequently categorized according to the components of anions; for example, oxides, sulfides, nitrides and fluorides. Therefore, most studies on the inorganic compounds are carried out in each category changing cation species. Moreover, several cations are often included in the compounds, so to speak, as mixed-cation compounds. In contrast, layered oxychalcogenides treated in this study are mixed-anion compounds including two anions, oxygen and chalcogen anions. Cations in oxychalcogenides are usually surrounded by both the oxygen and chalcogen anions. However, in the layered oxychalcogenides consisting of oxide and chalcogenide layers, the chalcogen anions surround specific cations exclusively [1-6]. Therefore, these compounds are called oxide chalcogenides as well as oxychalcogenides. Similar layered structures are also found in oxypnictides, fluorochalcogenides, fluoropnictides [7-10].

This unique layered structure may simply lead us to an idea that the layered oxychalcogenides have physical properties derived from either the oxide layers or chalcogenide layers; wide-gap and insulating properties of oxides or narrow-gap and semiconducting properties of chalcogenides. Therefore, consideration of the electronic structure in the layered oxychalcogenides provides us a more quantitative insight into their physical properties along with various electrical and optical measurements.

In this paper, several layered oxychalcogenides are chosen and shown as wide-gap semiconductors reviewing the concept of the materials design for wide-gap conductive oxides and oxychalcogenides [11-15]. Examining their electronic structures by energy band calculations and normal/inverse photoemission spectroscopy, recent new aspects of these materials originating from their unique layered crystal structure are discussed along with optical demonstrations of two-dimensional features.

Materials design and candidate materials for wide-gap semiconductors

Most typical wide-gap oxides such as MgO and Al_2O_3 are electrical insulators. However, there are exceptions such as ZnO and In_2O_3, which show *n*-type electrical conduction by appropriate doping. The electrical conduction in these wide-gap oxides basically originate from two conditions; high mobility of carriers and proper doping for carrier generation. In the search of new wide-gap or transparent conducting oxides, it was proposed that the materials satisfying the former condition can be designed by selecting appropriate component elements and crystal structures.

In the case of n-type materials, it is essential that the materials include *p*-block heavy cations with s^0 electronic configuration as major component elements. Namely, Zn^{2+}, Cd^{2+}, Ga^{3+}, In^{3+}, Sn^{4+} etc are crucial elements for wide-gap n-type conducting oxides. In addition, these ions

should be located in the crystal structure as close as possible to overlap their *s* orbitals with each other. Since the *s* orbitals form the conduction band, carrier electrons can be more mobile as the orbitals overlap increasingly. In our research, edge-sharing octahedra, “rutile chains”, are considered to be a favorable structural unit for *n*-type conduction [11,12].

Crystal structures of oxides are often described as packing of anion’s spheres. This description implies that electrons in the anion’s spheres, namely oxygen $2p^6$ orbital, are strongly localized. Since the closed shell of the oxygen $2p^6$ orbitals forms the valence band in the typical oxides, it is natural that *p*-type conduction hardly occurs in oxides. Therefore, an increase of covalency in the valence band is required to cause *p*-type conduction in oxides. The materials design of the wide-gap *p*-type conducting oxides is based on the concept that a Cu^+ ion is an essential element and the chemical bonds of Cu-O form a covalent hybridized band between oxygen $2p^6$ and Cu $3d^{10}$ orbitals at the top of the valence band. The covalency in the Cu-O bonds causes the delocalization of positive holes at the valence band maximum [13,14].

These concepts for wide-gap *p*-/*n*-type conducting oxides are applicable to chalcogenides such as sulfides and selenides. However, chalcogenides usually show much narrower energy gap than oxides. Therefore, we extended the concepts from oxides not to chalcogenides but oxychalcogenides, especially layered oxychalcogenides, to keep the wide-gap feature in these materials. The essences of the extended concepts for wide-gap oxychalcogenide semiconductors are illustrated in figure 1. The ions with s^0 orbitals such as Cd^{2+} and Sn^{4+} are indispensable for *n*-type conduction and the hybridization of chalcogen (Ch) p^6 and Cu $3d^{10}$ orbitals at the top of the valence band is vital for *p*-type conduction [15].

We selected several layered oxychalcogenides as candidates for wide-gap *p*-type and *n*-type semiconductors (Figure 2). These layered oxychalcogenides have unique crystal structural features that oxide and chalcogenide layers are clearly separated in the layered structures. The candidate materials for *p*-type semiconductors are LaCuOS, LaCuOSe, $Sr_2Cu_2ZnO_2S_2$ (SCZOS), and $Sr_2Cu(Ga/In)O_3S$ (SCGOS/SCIOS) [1-6]. These materials have common $(Cu_2Ch_2)^{2-}$ layers in the layered structure, and the $(Cu_2Ch_2)^{2-}$ layers are intervened by the oxide layers with ionic cations such as La and Sr ions. Since the Cu-Ch bonds in the $(Cu_2Ch_2)^{2-}$ layers are considered to form hybridized states at the valence band maximum (VBM), *p*-type electrical conduction is anticipated in these materials. The candidate materials for *n*-type semiconductors are $La_2CdO_2Se_2$ and $La_2SnO_2S_3$ [2], in which $(CdSe_2)^{2-}$ or $(SnS_3)^{2-}$ layers are separated by $(La_2O_2)^{2+}$ layers. Since these materials include Cd^{2+} or Sn^{4+} ions as major components, a large overlap of their s orbitals and *n*-type electrical conduction are expected in the $(CdSe_2)^{2-}$ or $(SnS_3)^{2-}$ layers. In both *p*-type and *n*-type cases, the chalcogenide layers are considered to be carrier conduction paths and the oxide layers are to give wide-gap properties to these materials.

Basic optical and electrical properties of layered oxychalcogenides

The layered oxychalcogenides are usually synthesized by solid-state reactions in evacuated silica glass tubes to prevent the evaporation of chalcogen elements. The details of sample preparation were reported elsewhere [16-20]. Each obtained sample was confirmed to be a single phase by X-ray powder diffraction measurements.

Figure 3 shows diffuse reflectance spectra of the samples. Since the diffuse reflection spectra of powder samples are often interpreted as the transmission spectra of small crystals, fundamental absorption edges or energy gaps of samples are approximately estimated from the onset of sharp reflectance drop in the spectra. All samples show the energy gaps larger than 2 eV and the energy gaps of most La oxychalcogenides exceed to 3 eV indicating a transparent feature in the visible region. As for the candidate materials for wide-gap *p*-type semiconductors, the energy gap of LaCuOS and LaCuOSe are 3.1 and 2.8 eV, respectively [17]. The oxyselenide shows a smaller energy gap than the oxysulfide because the valence band maximum in the oxyselenide is shallower than the oxysulfide with respect to the vacuum level. The energy gaps of Sr-Cu-M-O-S system (M=Zn, Ga, In) are in the range from 2.7 to 2.3 eV and these values are smaller than those for LaCuOCh (Ch=S and Se). Since the valence band structure are similar between these Sr and La oxysulfides, differences in the conduction band structure cause the smaller band gap in the Sr-Cu-M-O-S system [18]. In the case of the candidates for wide-gap *n*-type semiconductors, both $La_2CdO_2Se_2$ and $La_2SnO_2S_3$ show the energy gap larger than 3 eV. In spite of including Se ions, $La_2CdO_2Se_2$ shows the largest energy gap (3.3 eV) among these oxychalcogenides. This widest gap in $La_2CdO_2Se_2$ probably originates from the local structure in the $(CdSe_2)^{2-}$ layers, which consist of vertex sharing $CdSe_4$ tetrahedra chains [20].

Electrical conductivities of sintered samples were measured and typical data are shown in Figure 4. Non-doped LaCuOS shows semiconducting properties and Sr substitution at La sites remarkably increases the conductivity converting the semiconducting conduction into degenerate conduction. Similar behavior was observed in LaCuOSe. The Sr substitution at La sites effectively generates hole carriers in La oxychalcogenides. SCZOS is slightly conductive in a non-doped state. However, the conductivity was enhanced by Na substitution at Sr sites. SCGOS/SCIOS shows similar behavior but SCIOS was less conductive than SCZOS/SCGOS. The Seebeck coefficients of all samples including the $(Cu_2Ch_2)^{2-}$ layers were positive values, which indicate that LaCuOCh and Sr-Cu-M-O-S (M=Zn, Ga and In) oxysulfides are *p*-type conductors. The hole mobilities of LaCuOCh thin film samples were 0.2-0.5 $cm^2V^{-1}s^{-1}$ for LaCuOS and 4-8 $cm^2V^{-1}s^{-1}$ for LaCuOSe in semiconducting or degenerate semiconducting states [21-23]. In contrast to these wide-gap *p*-type oxychalcogenides, the conductivities of $La_2CdO_2Se_2$ and $La_2SnO_2S_3$ were significantly small. $La_2CdO_2Se_2$ was insulating and $La_2SnO_2S_3$ were very slightly conductive. Although Al-doping and Nb/Sb-doping were

attempted against $La_2CdO_2Se_2$ and $La_2SnO_2S_3$, respectively, the conductivities do not increase more than non-doped states. $La_2SnO_2S_3$ showed a negative Seebeck coefficient of –40 mVK^{-1} revealing that the conduction in La_2SnO_2S is at least *n*-type. This low *n*-type conductivity may result from carrier compensation by lattice defects.

The basic optical and electrical properties of the layered oxychalcogenides revealed that these materials were wide-gap *p*-/*n*-type semiconductors. However, the *n*-type materials are much less conductive than the *p*-type ones. Further materials development and improvement of doping techniques are necessary in future research. Since LaCuOCh is chemically stable at room temperature, this material is the most promising material for wide-gap *p*-type semiconductors among these oxychalcogenides. Hereafter, LaCuOCh is mainly taken up as a prototype of the layered oxychalcogenides and its electronic structure and advanced optoelectronic properties are examined.

Electronic structures of LaCuOCh layered oxychalcogenides

Electronic structures of LaCuOCh (Ch=S, Se and Te) were examined by normal/inverse photoemission spectroscopy (PES/IPES) and energy band calculations. PES measurements were conducted using a discharged lamp (VG) that emitted the excitation lines of He II (40.8 eV), He I (21.2 eV), and Ne I (16.7 eV). The surfaces of the samples were scraped with a diamond file under a vacuum of $8x10^{-10}$ Torr to obtain clean surfaces before each measurement. The energy band structures of LaCuOCh (Ch=S, Se and Te) were calculated by the ABCAP code of a full-potential linearized augmented plain-wave (FLAPW) method. The FLAPW calculations based on density functional theory were performed using a local density approximation (LDA) with an on-site correlation for La 4f electrons. The total density of states (DOS) and partial DOS (PDOS) were calculated to compare with the PES spectra [24].

Figure 5 shows PES/IPES spectra of $LaCuOS_{1-x}Se_x$ (x=0.0, 0.5, 1.0). Five bands, A to E, were observed in the valence band and two bands, X and Y, were in the conduction band. The conduction band structures were similar between LaCuOS and LaCuOSe, while the valence band structures were different between them. Therefore, the valence band structures were analyzed in detail along with the energy band calculations. In the analysis, the background in the UPS spectra was subtracted smoothly. To compare the PES spectra with the calculated electronic structure, the VBM in each spectrum was accurately aligned at the binding energy of E_B =0 eV and the origin of the energy scale in the calculated DOS and PDOS was set at the VBM. Moreover, a smearing treatment was added to the DOS/PDOS as shown in Figure 5.

The UPS spectra of LaCuOS measured using the excitation lines of He II (40.8eV), He I (21.2eV), and Ne I (16.7eV) are shown in Figure 6 along with the total DOS and PDOS. The intensities of the UPS spectra are normalized at a binding energy where the PDOS of Cu 3*d*

states is maximized, approximately at 3 eV. The intensity of the photoemission spectra usually depends on the photoionization probability of the atoms [25]. Therefore, the data on the photoionization cross sections (σ) of the atomic orbitals is important when interpreting the shape of the photoemission spectra. The σ of Cu 3*d* orbital slightly decreases (9.944 Mb/atom for He II, 7.285 for He I and 6.284 for Ne I), while the σ of O 2*p* orbital gradually increases (6.816 Mb/atom for He II, 10.69 for He I and 10.43 for Ne I) as the excitation energy decreases. The values indicate that the variations against the excitation energy for these two orbitals are relatively small. On the other hand, the cross sections of the S 3*p* orbitals are strongly enhanced (0.6051 Mb/atom for He II, 4.371 for He I and 18.25 for Ne I) as the excitation energy decreases. This large excitation energy dependence of σ in the S 3*p* orbitals is considerably different from those in the Cu 3*d* and O 2*p* orbitals.

In figure 6, Band A is right below the VBM and its intensity increases as the excitation energy decreases. This excitation energy dependence suggests that Band A includes components from the S 3*p* states. Since the calculated PDOSs show that Band A is mainly composed of the Cu 3*d* and S 3*p* states, Band A is assigned to a Cu 3*d* - S 3*p* anti-bonding band. Band B is located at a binding energy of approximately 3.0 eV, which is due to the Cu 3*d* non-bonding band since the PDOS maximum of the Cu 3*d* states is also located at this energy. Band C is assigned to the S 3*p* - Cu 3*d* bonding band, which forms the counterpart to Band A. The intensity of Band C is strongly enhanced as the excitation energy decreases and corresponds to the increase in the photoionization cross section of the S 3*p* orbitals. The PDOSs of S 3*p* and Cu 3*d* states show overlapped bands at the energy for Band C. Bands C and D happen to be located at almost the same energy in LaCuOS. A broad band indexed as D is observed at the same energy as Band C in the He II UPS spectrum, although the photoionization cross section of the S 3*p* orbitals is negligible in the He II radiation. Since the PDOS of the O 2p and La 5d states appears at the same energy for Band D, Band D is assigned to the O 2*p* - La 5*d* bonding band. The O 2p states are dominant in Band D because the PDOS of the La 5*d* states is much smaller than that of the O 2p states. Band E is located at the bottom of the VB. Band E intensities increase as the excitation energy decreases and noticeable S 3*p* states seen in the PDOS correspond to Band E. Because the Cu 4*s*, 3*d* states and the S 3*p* states, are clearly observed in the energy for Band E, this band is assigned to the S 3*p* - Cu 4*s*, 3*d* bonding bands.

The band assignment for LaCuOSe and LaCuOTe is similarly conducted interpreting the origin of the five bands in the valence band. Figure 7 shows the He II UPS spectra and the total DOSs for a series of LaCuOCh (Ch=S, Se and Te). The width of Band A assigned to the Ch *p* - Cu 3*d* anti-bond band become larger in both the UPS spectra and total DOS in the order of LaCuOS, LaCuOSe and LaCuOTe, suggesting that the hybridization between Ch *p* and Cu 3*d* increases in the same order. The shape of Band B assigned to the Cu 3*d* non-bonding band is

very similar among LaCuOCh, but the energy position shifts slightly deeper in the binding energy from LaCuOS to LaCuOTe. Bands C and D assigned to the Ch *p* - Cu 3*d* and the O 2*p* - La 5*d* bonding bands, respectively, are at the same energy in LaCuOS and are separate in LaCuOSe and LaCuOTe since Band C shifts to a smaller binding energy while Band D goes to a larger binding energy. The separation between Bands C and D in LaCuOTe is larger than that in LaCuOSe. Band E is located at the bottom of the valence band and significant differences were not observed between LaCuOCh.

The experimental analysis of the conduction band is rather difficult due to the broad feature of the IPES spectra. Therefore, the conduction band structure is analyzed on the basis of the results of the energy band calculations. Figure 8 shows the calculated band structure near the energy gap for LaCuOS. From the DOS/PDOS, it is understood that the conduction band near the bandgap is mainly composed of Cu 4*s* and La 5*d* states and the Cu 4*s* states are below the La 5*d* states.

The band structure examined above indicates that the both the conduction band minimum (CBM) and VBM originate from Cu and S states as shown in Figure 8. Namely, the energy gap in these materials are determined by the $(Cu_2Ch_2)^{2-}$ layers. Therefore, carriers generated in this material are confined both energetically and spatially into the chalcogenide layers. This crystal and electronic structure bring unique optoelectronic properties to the layered oxychalcogenides.

Optoelectronic properties originating from layered structures

First of all, it is noteworthy that the bandgap of LaCuOS is a direct-type and electronic transition between CBM and VBM is allowed in this material as shown in the energy band diagram in figure 8. Actually, excitonic absorption and emission were observed in this material even at room temperature [26]. Due to these features, LaCuOS was revalued from a simple wide-gap *p*-type conducting materials to a unique wide-gap *p*-type semiconductor.

The uniqueness of the layered oxychalcogenides arises from correlations between their layered crystal structure and electronic structure. The correlations provide the layered oxychalcogenides with two contrasting pictures. The first picture is built-in multiple quantum wells (MQWs) formed with chalcogenide and oxide layers; the $(Cu_2S_2)^{2-}$ layer works as a well and the $(La_2O_2)^{2+}$ layer serves as a barrier for hole carriers due to the large band offset energy at the valence band (figure 8). The other picture is 2D chalcogenide crystals or molecules embedded in an inert oxide matrix; the $(Cu_2S_2)^{2-}$ layer is considered as an isolated or independent crystal or molecule, which may be classified into nano-materials such as nano-crystals and nano-tubes. Figure 9 illustrates the two pictures schematically. Since these two pictures are considered to be just different ways of descriptions, the two contrastive views can be realized in a particular crystal structure such as the layered oxychalcogenides.

The picture of the MQW structure was experimentally confirmed by optical absorption spectra measured on high-quality epitaxial thin films of $LaCuOS_{1-x}Se_x$ and LnCuOS (Ln=La, Pr and Nd) [27]. The epitaxial films of 150 nm thickness were grown on MgO single crystal substrates by reactive solid-phase epitaxy [28, 29]. Measurements were conducted at 10 K using a conventional spectrometer with a cryostat. Figure 10 shows the optical absorption spectra of $LaCuOS_{1-x}Se_x$ ($0 \leq x \leq 1$) above the fundamental absorption edges. A pair of sharp absorption peaks (n=1) due to excitons is observed at the absorption edge in each film. The energy spacing between the peak pairs increases as the Se content increases and reaches a maximum splitting of 125 meV for LaCuOSe (x=1). Anion substitution by Te^{2-} further enhanced the peak splitting up to 220 meV in $LaCuOSe_{0.6}Te_{0.4}$. The increase in the splitting with atomic number of Ch ions and the symmetry analysis of the VBM lead to the conclusion that the splitting results from the spin-orbit interaction of Ch ions.

This spin-orbit splitting at the VBM enabled clear step-like shapes to be observed in optical absorption spectra, especially for LaCuOSe. This step-like absorption confirms that these compounds have two-dimensional density of states (DOS). Therefore, the step-like increase in the absorption spectra of LnCuOCh is interpreted as overlapping two step-like DOSs split by the spin-orbit interaction (Figure 10). A sharp exciton peak at the step edge accompanies each step structure as observed similarly in artificial MQWs fabricated from III-V or II-VI compound semiconductors. The splitting due to the spin-orbit interactions by Ln (Ln=Pr, Nd) ions is also seen in LnCuOS although the splitting is rather small compared to that of the Ch ions.

The other picture as a 2D chalcogenide crystal or molecule is based on the viewpoint that the $(La_2O_2)^{2+}$ and $(Cu_2Ch_2)^{2-}$ layers in LaCuOCh interact only electrostatically as if they form donor - acceptor pairs of molecules in the crystal. The obvious layered structure support this picture because the La - Ch distance is much larger than the simple sum of these ionic radii suggesting that covalent bonding is negligible between the layers. Therefore, considering the chalcogenide layer as a 2D crystal/molecule, we compared the optical properties of the layered oxychalcogenides with those of nanoparticles of related chalcogenides. Since the optical properties of Cu_2S or Cu_2Se nanoparticles are not available to date, a comparison between $La_2CdO_2Se_2$ and CdSe nanoparticles was performed. These two materials have similar local structure around Cd ions; four Se ions coordinate to a Cd ion forming a $CdSe_4$ tetrahedron and each tetrahedron is connected sharing their vertexes. Although the way of the vertex sharing connection is different between $La_2CdO_2Se_2$ and CdSe, the neighboring Cd – Cd and Se – Se distances (both are 0.41 nm) in $La_2CdO_2Se_2$ are almost the same as those in CdSe (0.43 nm). The conduction band and valence band in $La_2CdO_2Se_2$ were formed with the Cd 5*s* and Se 4*p* states, respectively, indicating that the band gap of this material is determined by the $(CdSe_2)^{2-}$ layers [30].

It is known that the band gap energy of CdSe nanoparticles varies depending on the size of the particles. This energy dependence on the particle size is interpreted as a quantum size effect, visualizing the particle as a quantum dot [31]. Figure 11 shows the variation of the absorption edge energy in CdSe nanoparticles [32]. The band-gap energy of CdSe nanoparticles increases from 1.8 eV (three-dimensional bulk) to 2.9 eV (zero-dimensional nanocrystals), approaching the band-gap energy of $La_2CdO_2Se_2$ (~3.3 eV). The band-gap energy of $La_2CdO_2Se_2$ is as large as that of CdSe nanoparticles with a particle size of ~1 nm, which is close to the thickness of the $(CdSe_2)^{2-}$ layers. This coincidence suggests that the quantum effect may be also occurred in the $(CdSe_2)^{2-}$ layers and the effect may result in the large band-gap of $La_2CdO_2Se_2$. Another two-dimensional feature in $La_2CdO_2Se_2$ is observed as the large binding energy of excitons generated in the $(CdSe_2)^{2-}$ layers. Table 1 demonstrates that the exciton binding energy of the CdSe-based material increases as the dimensionality decreases [33-35]. A large value of 42 meV, which is comparable to that of $La_2CdO_2Se_2$, is obtained for the CdSe/CdS superlattice (two-dimensional excitons). Therefore, it is considered that the large binding energy of exciton in $La_2CdO_2Se_2$ comes from the exciton confinement effect in the $(CdSe_2)^{2-}$ layers. These evident two dimensional features observed in the band gap energy and exciton binding energy suggest that each $(CdSe_2)^{2-}$ layer may be treated as an isolated 2D chalcogenide crystal or molecule in the layered crystal structure.

The two pictures of the layered oxychalcogenides suggested in figure 9 were examined and demonstrated using typical materials such as LaCuOCh and $La_2CdO_2Se_2$. Since these features originate from the unique layered structures, it is suggested that similar features will be observed in other layered materials such as oxypnictides, fluorochalcogenides and fluoropnictides if the component elements are properly selected.

Summary

The concept of materials design for wide-gap conductive oxides and oxychalcogenides was shown, and according to the concept, p-type and n-type layered oxychalcogenides were presented as wide-gap semiconductors. Both type of materials consist of two layers with different chemical bonding; oxide layers including ionic elements and chalcogenide layers containing covalent elements, such as Cu and Cd. These two oxide and chalcogenide layers in the unique layered structure is considered to provide wide-gap and conductive properties to these materials, respectively. Analyzing the electronic structures of these compounds, it was proposed that the layered structures can be visualized as natural multiple quantum wells consisting of the oxide and chalcogenide layers or 2D chalcogenide crystals/molecules embedded in an oxide matrix. These two contrastive pictures were demonstrated experimentally, showing step-like absorption edges and large energy gap and exciton binding energy due to

quantum effects. These interesting features found in the layered oxychalcogenides will be extended to other layered materials such as oxypnictides and fluoropnictides in future research, along with studies for application of these materials to optoelectronic devices.

References

[1] M. Palazzi, Acad. Sci., Paris, C. R. **292** (1981) 789

[2] M. Guittard, S. Benazeth, J. Dugué, S. Jaulmes, M. Palazzi, P. Laruelle and J. Flahaut, J. Solid State Chem. **51** (1984) 227

[3] W. J. Zhu and P. H. Hor, J. Solid State Chem. **130** (1997) 319

[4] W. J. Zhu and P. H. Hor, Inorg. Chem. **36** (1997) 3576

[5] W. J. Zhu and P. H. Hor, J. Solid State Chem. **134** (1997) 128

[6] W. J. Zhu, Y. Z. Huang, C. Dong and Z. X. Zhao, Mater. Res. Bull. **29**, 143 (1994)

[7] A. T. Nientiedt and W. Jeitschko, Inorg. Chem. **37** (1998) 386

[8] W. J. Zhu, Y. Z. Huang, F. Wu, C. Dong H. Chen and Z. X. Zhao, Mater. Res. Bull. **29**, 505 (1994)

[9] C. H. Park, D. A. Keszler, H. Yanagi and J. Tate, Thin Solid Films **445** (2003) 288

[10] L. Cario, H. Kabbour and A. Meerschaut, Chem. Mater. **17** (2005) 234

[11] H. Kawazoe, N. Ueda, H. Un'no, T. Omata, H. Hosono and H. Tanoue, J. Appl. Phys. **76** (1994) 7935

[12] H. Kawazoe and K. Ueda, J. Am. Ceram. Soc. **82** (1999) 3330

[13] H. Kawazoe, M. Yasukawa, H. Hyodo, M. Kurita, H. Yanagi and H. Hosono, Nature **389** (1997) 939

[14] H. Kawazoe, H. Yanagi, K. Ueda and H. Hosono, MRS Bull. **25** (2000) 28

[15] K. Ueda, K. Takafuji, H. Hiramatsu, H. Ohta, M. Hirano, H. Hosono and H. Kawazoe, Mat. Res. Soc. Symp. Proc. **747** (2003) V2.1.1

[16] K. Ueda, S. Inoue, S. Hirose, H. Kawazoe and H. Hosono, Appl. Phys. Lett. **77** (2000) 2701

[17] K. Ueda and H. Hosono, J. Appl. Phys. **91** (2002) 4768

[18] K. Ueda, S. Hirose, H. Kawazoe and H. Hosono, Chem. Mater. **13** (2001) 1880

[19] K. Ueda, K. Takafuji, H. Hiramatsu, H. Ohta, T. Kamiya, M. Hirano and H. Hosono, Chem. Mater. **15** (2003) 3692

[20] H. Hiramatsu, K. Ueda, T. Kamiya, H. Ohta, M. Hirano and H. Hosono, J. Mater. Chem. **14** (2004) 2946

[21] H. Hiramatsu, M. Orita, M. Hirano, K. Ueda and H. Hosono, J. Appl. Phys. **91** (2002) 9177

[22] H. Hiramatsu, K. Ueda, H. Ohta, M. Hirano, T. Kamiya and H. Hosono, Appl. Phys. Lett. **82** (2003) 1048

[23] H. Hiramatsu, K. Ueda, K. Takafuji, H. Ohta, M. Hirano, T. Kamiya and H. Hosono, Appl. Phys. A **79** (2004) 1521

[24] K. Ueda, H. Hosono, N. Hamada, J. Phys.: Condens. Matter **16** (2004) 5179

[25] J. J. Yeh, *Atomic Calculation of Photoionization Cross-Sections and Asymmetry*

Parameters (London: Gordon and Breach) 1993

[26] K. Ueda, S. Inoue, H. Hosono, N. Sarukura and M. Hirano, Appl. Phys. Lett. **78** (2001) 2333

[27] K. Ueda, H. Hiramatsu, H. Ohta, M. Hirano, T. Kamiya and H. Hosono, Phys. Rev. B **69** (2004) 155305

[28] H. Hiramatsu, K. Ueda, H. Ohta, M. Orita, M. Hirano and H. Hosono, Appl. Phys. Lett. **81** (2002) 598

[29] H. Hiramatsu, H. Ohta, T. Suzuki, C. Honjo, Y. Ikuhara, K. Ueda, T. Kamiya, M. Hirano and H. Hosono, Cryst. Growth Des. **4** (2004) 301

[30] H. Hiramatsu, K. Ueda, T. Kamiya, H. Ohta, M. Hirano and H. Hosono, J. Phys. Chem. B **108** (2004) 17344

[31] In the infinite confinement limit, the apparent absorption edge energy (*E*) becomes $E=E_g+h^2/(8mR^2)$ for zero-dimensional confinement and $E=E_g+h^2/(8m_zL_z^2)$ for two-dimensional confinement, where E_g, h, R or L_z, and m or m_z denote band gap energy, Planck constant, confinement size, and an effective mass for electrons and holes, respectively.

[32] C. B. Murray, D. J. Norris, M. G. Bawendi, J. Am. CHem. Soc. **115** (1993) 8706

[33] J. O. Dimmock, R. G. Wheeler, J. Appl. Phys. **32** (1961) 2271

[34] R. G. Wheeler, J. O. Dimmock, Phys. Rev. **125** (1962) 1805

[35] K. P. O'Donnell, P. J. Parbrook, B. Henderson, C. Trager-Cowan, X. Chen, F. Yang, M. P. Halsall, P. J. Wright, B. Cockayne, J. Cryst. Growth **101** (1990) 554

Table 1 Energy gap and exciton binding energy of layered oxychalcogenides and their related materials

Materials	E_g (eV)	E_b (meV)
$La_2CdO_2Se_2$	3.3	40
CdS single crystal (3D)	1.8	15
CdSe/CdS superlattice (2D)	—	42
CdSe nanocrystals (0D)	2.9	—
LaCuOS	3.1	50
LaCuOSe	2.8	50
Cu_2S	1.1	—
$CuGaS_2$	2.48	20

Figure Captions

Figure 1 Schematic molecular diagram of oxychalcogenides (left) and schematic energy band diagram along with the overlap of atomic orbitals (right). The caions with large s^0 orbitals are indispensable for n-type conduction and the hybridization of chalcogen (Ch) p^6 and Cu $3d^{10}$ orbitals is vital for p-type conduction to disperse the conduction/valence band or to form conduction paths in crystals.

Figure 2 Crystal structures of typical layered oxychalcogenides, LaCuOS and $La_2CdO_2Se_2$, which are candidates for wide-gap *p*- and *n*-type semiconductors, respectively.

Figure 3 Diffuse reflectance spectra of layered oxychalcogenides.

Figure 4 Electrical conductivities of $La_{1-x}Sr_xCuOS$, $Sr_{2-y}Na_yCu_2ZnO_2S_2$ and $La_2SnO_2S_3$ as a function of temperatures.

Figure 5 PES (He I) and IPES spectra of $LaCuOS_{1-x}Se_x$ (x=0.0, 0.5 and 1.0) along with the density of states for LaCuOSe. The PES spectra were measured using the excitation line of He I.

Figure 6 UPS spectra of LaCuOS examined using the excitation line of He I, He II and Ne I along with the total DOS and PDOS.

Figure 7 UPS (He II) spectra of LaCuOCh (Ch=S, Se and Te) along with each calculated DOS.

Figure 8 Energy band diagram and the total/partial DOS of LaCuOS near the Fermi energy (left) and the band off-set at the C.B. and V.B. (right).

Figure 9 Two views of layered oxychalcogenides relating to their crystal structures; MQW structures (left) and 2D chalcogenide crystals/molecules (right).

Figure 10 Optical absorption spectra of $LaCuOS_{1-x}Se_x$ near the absorption edges exhibiting step-like structure with exciton peaks at the step edges.

Figure 11　Variation of absorption edge energy in CdSe nanoparticles and the energy gap of CdSe (bulk), CuS/Se (bulk) and the related oxychalcogenides.

Figure 1

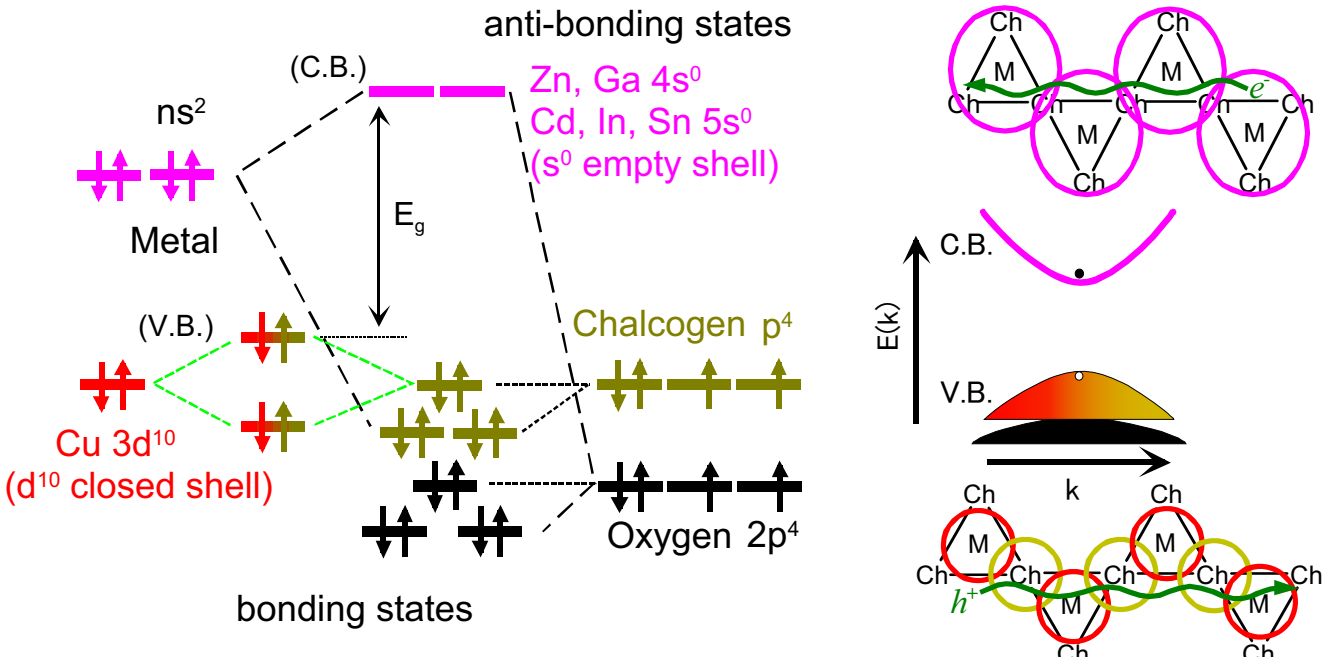
anti-bonding states
(C.B.)
Zn, Ga 4s0
Cd, In, Sn 5s0
(s0 empty shell)
ns2
Metal
Eg
(V.B.)
Chalcogen p4
Cu 3d10
(d10 closed shell)
Oxygen 2p4
bonding states
Ch
M
e-
C.B.
E(k)
V.B.
k
h+

Figure 2

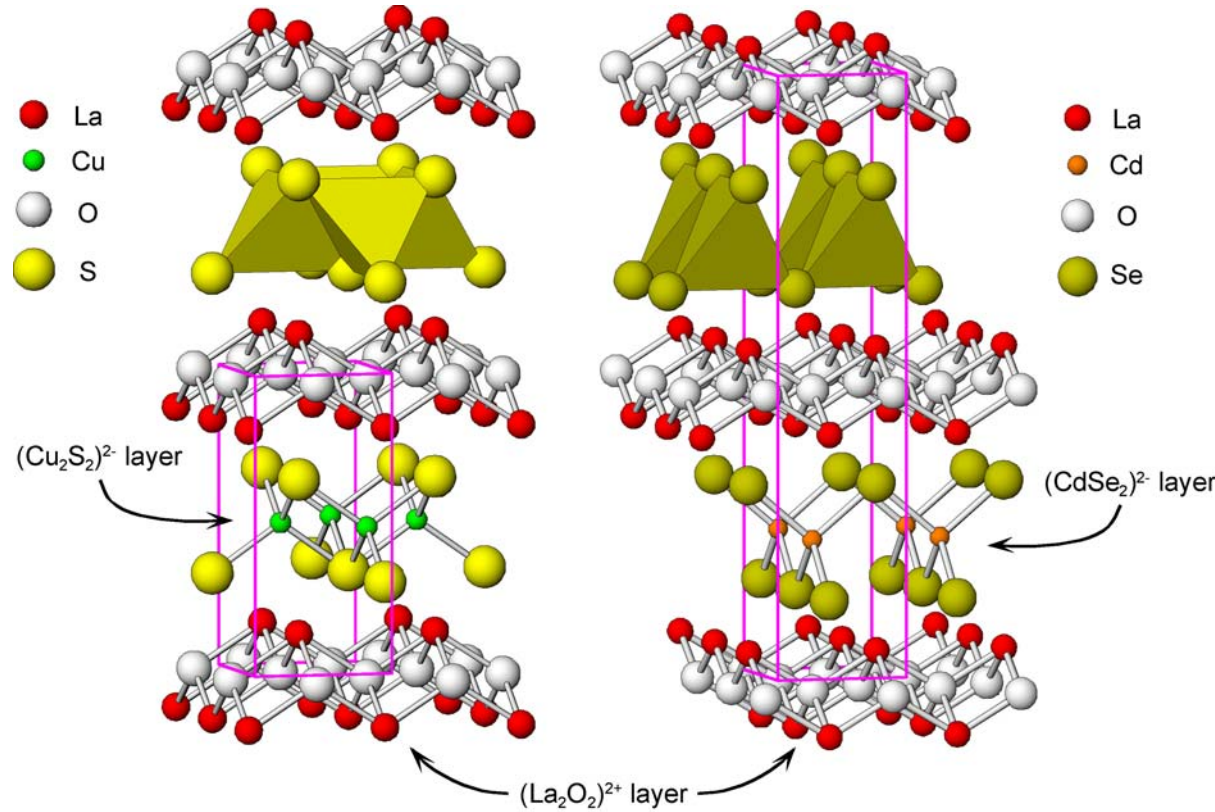

Figure 3

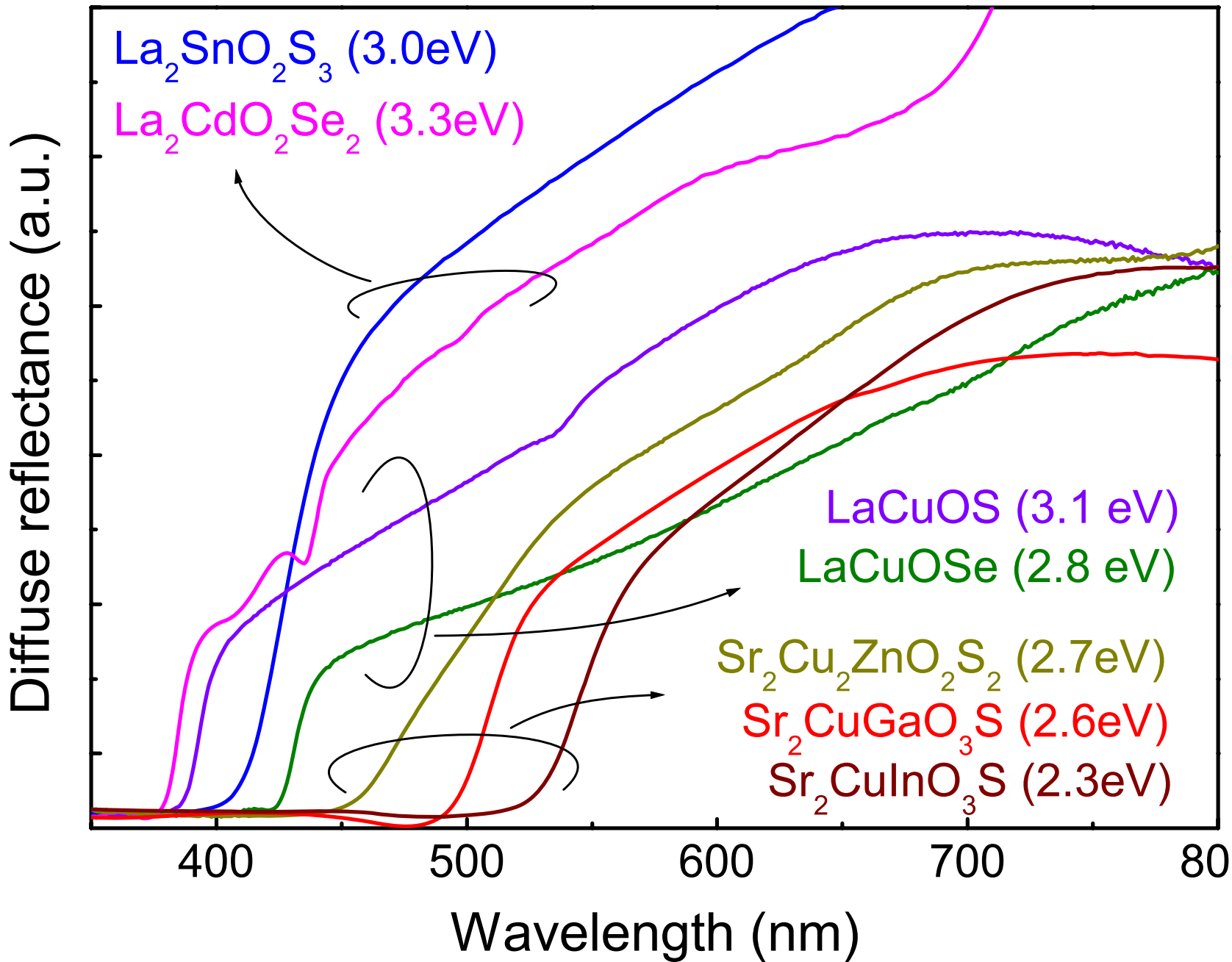
La2SnO2S3 (3.0eV)
La2CdO2Se2 (3.3eV)
LaCuOS (3.1 eV)
LaCuOSe (2.8 eV)
Sr2Cu2ZnO2S2 (2.7eV)
Sr2CuGaO3S (2.6eV)
Sr2CuInO3S (2.3eV)
Diffuse reflectance (a.u.)
400
500
600
700
800
Wavelength (nm)

Figure 4

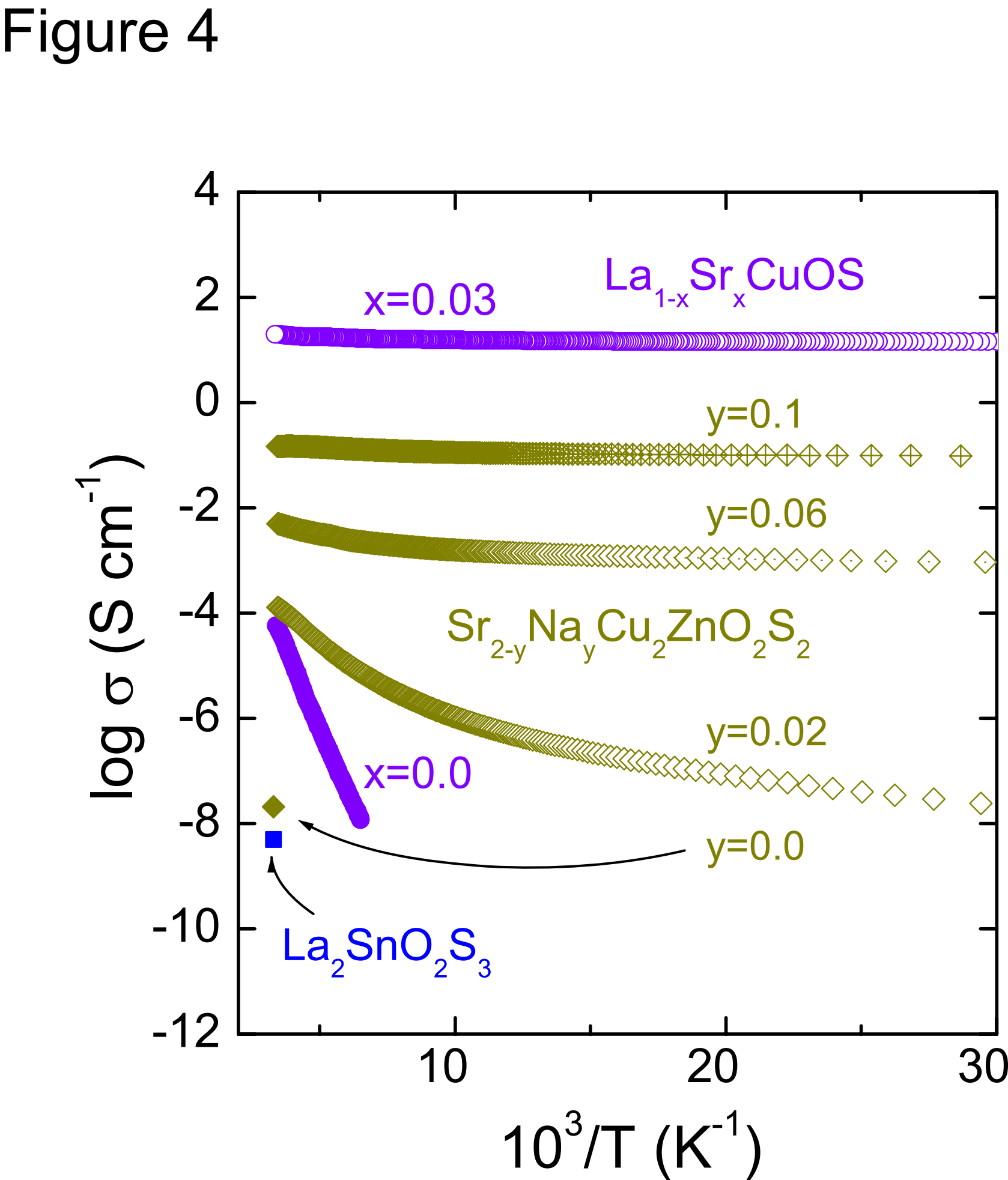
4
2
0
-2
-4
-6
-8
-10
-12
log σ (S cm-1)
10
20
30
10^3/T (K^-1)
La1-xSrxCuOS
x=0.03
y=0.1
y=0.06
Sr2-yNayCu2ZnO2S2
y=0.02
x=0.0
y=0.0
La2SnO2S3

Figure 5

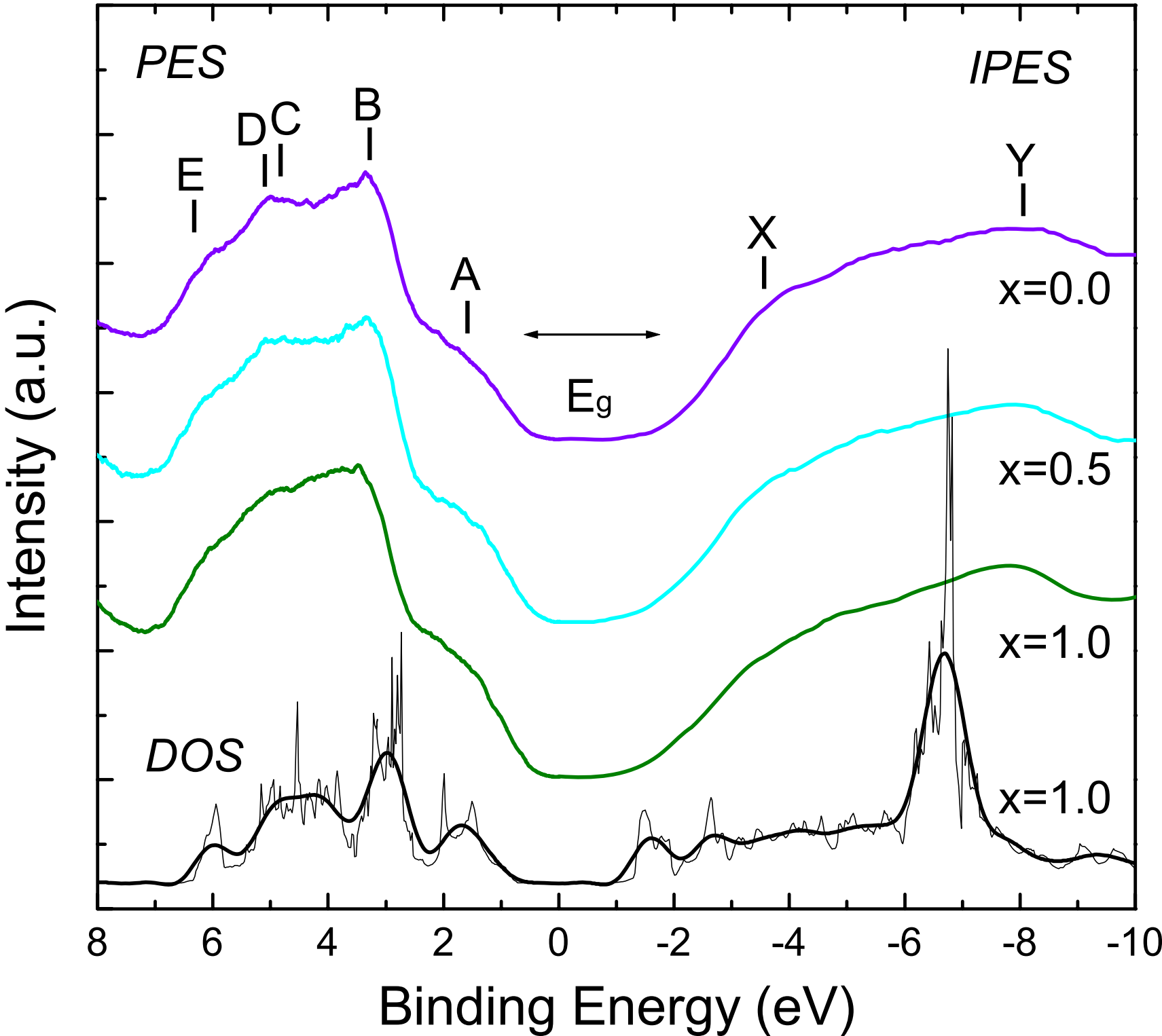
PES
IPES
E
D
C
B
A
X
Y
E_g
x=0.0
x=0.5
x=1.0
DOS
x=1.0
Intensity (a.u.)
8
6
4
2
0
-2
-4
-6
-8
-10
Binding Energy (eV)

Figure 6

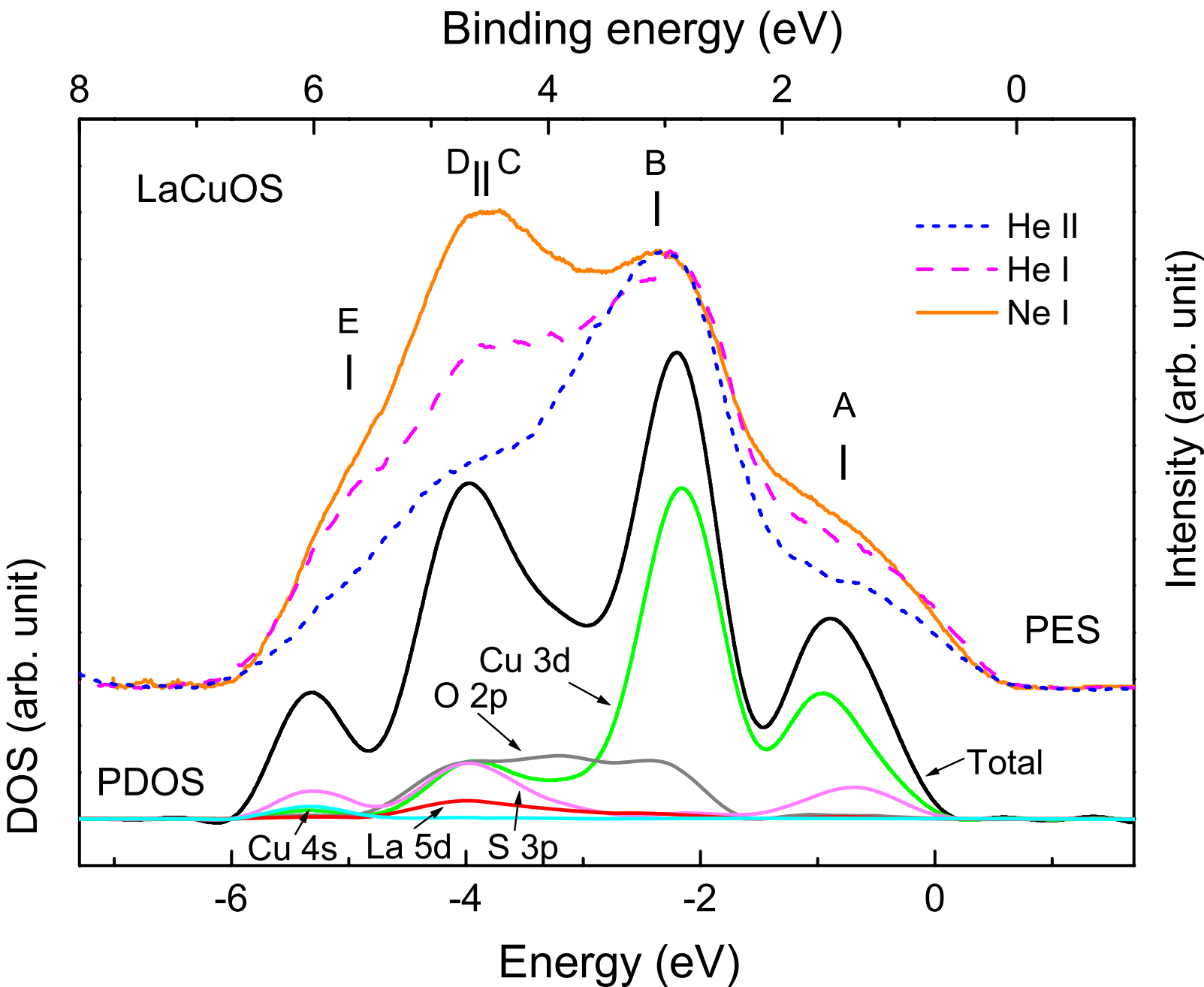
Binding energy (eV)
8
6
4
2
0
LaCuOS
D
C
B
E
A
He II
He I
Ne I
PES
PDOS
Cu 3d
O 2p
Total
Cu 4s
La 5d
S 3p
DOS (arb. unit)
Intensity (arb. unit)
-6
-4
-2
0
Energy (eV)

Figure 7

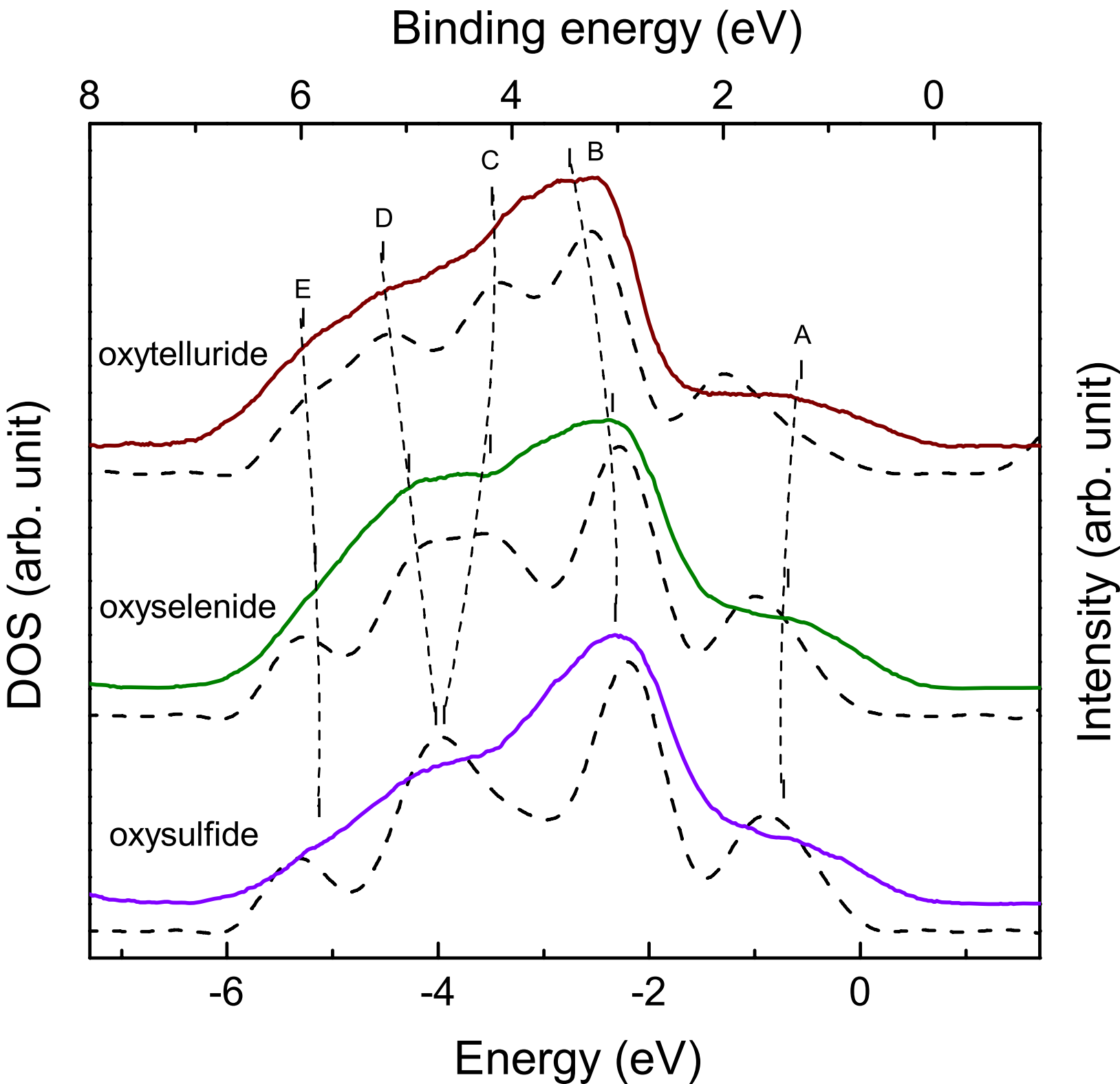
Binding energy (eV)
8
6
4
2
0
A
B
C
D
E
oxytelluride
oxyselenide
oxysulfide
DOS (arb. unit)
Intensity (arb. unit)
-6
-4
-2
0
Energy (eV)

Figure 8

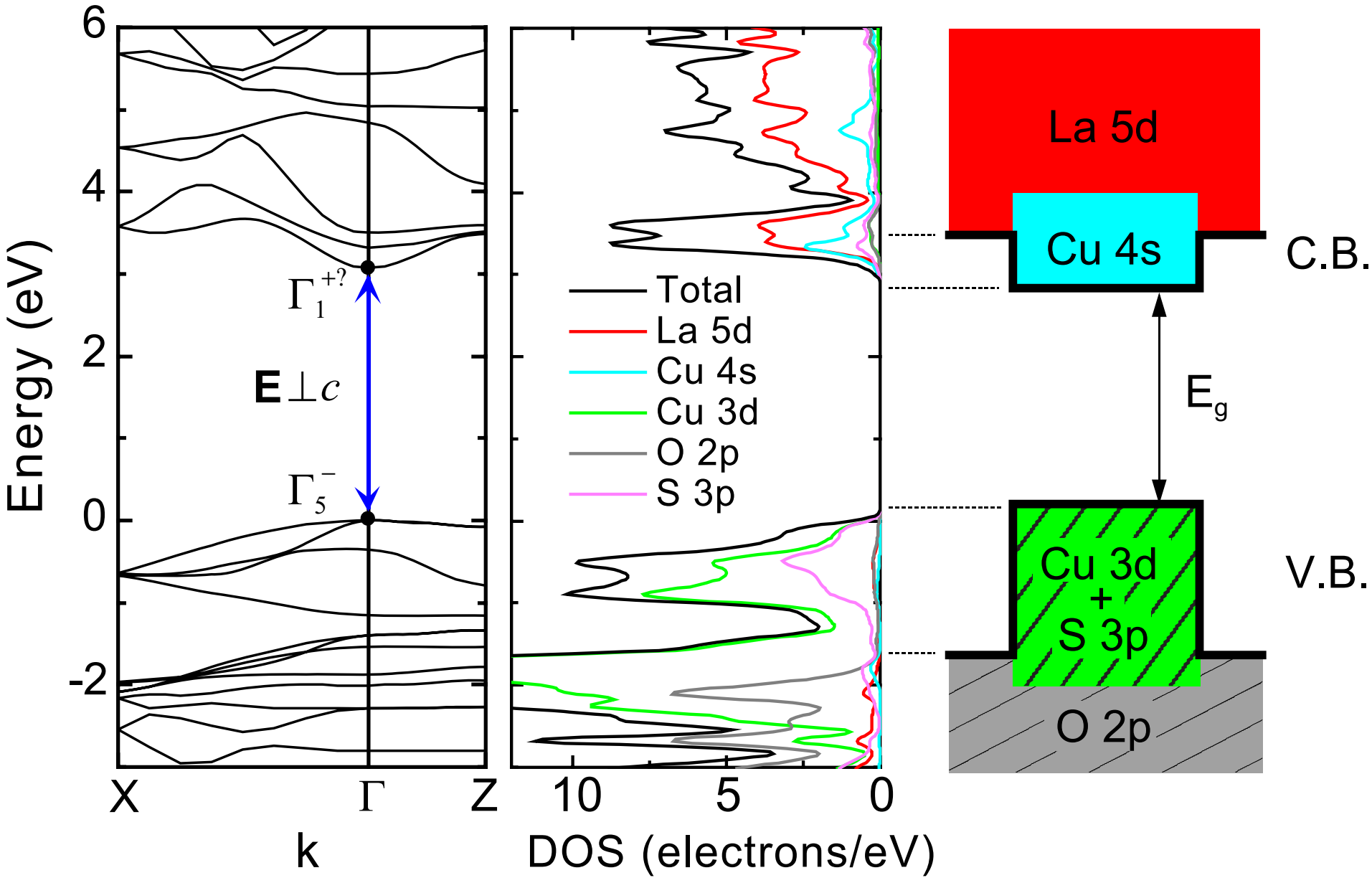
6
4
2
0
-2
Energy (eV)
X
Γ
Z
k
$\Gamma_1^{+?}$
E ⊥ c
Γ_5^-
Total
La 5d
Cu 4s
Cu 3d
O 2p
S 3p
10
5
0
DOS (electrons/eV)
La 5d
Cu 4s
C.B.
E_g
Cu 3d
+
S 3p
V.B.
O 2p

Figure 9

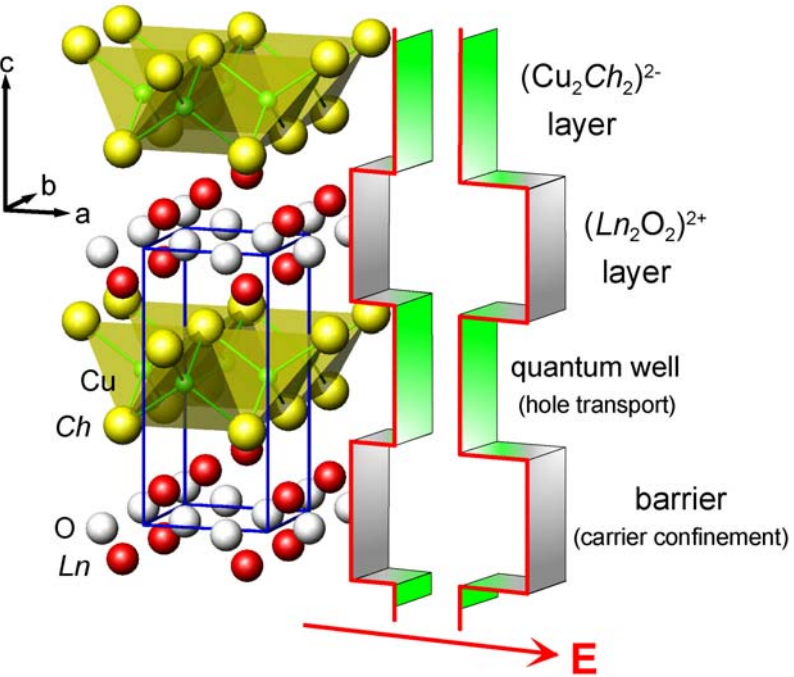
c
b
a
Cu
Ch
O
Ln
$(Cu_2Ch_2)^{2-}$
layer
$(Ln_2O_2)^{2+}$
layer
quantum well
(hole transport)
barrier
(carrier confinement)
E

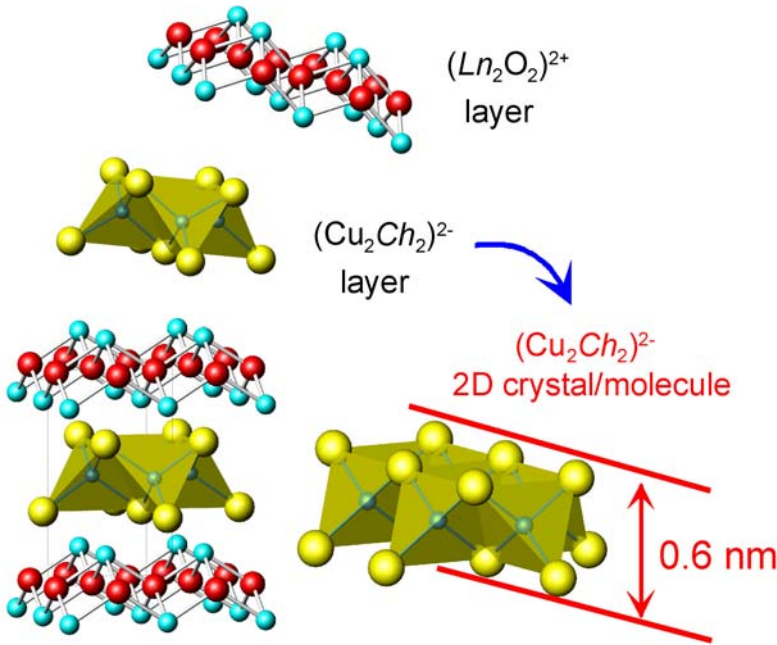
$(Ln_2O_2)^{2+}$
layer
$(Cu_2Ch_2)^{2-}$
layer
$(Cu_2Ch_2)^{2-}$
2D crystal/molecule
0.6 nm

Figure 10

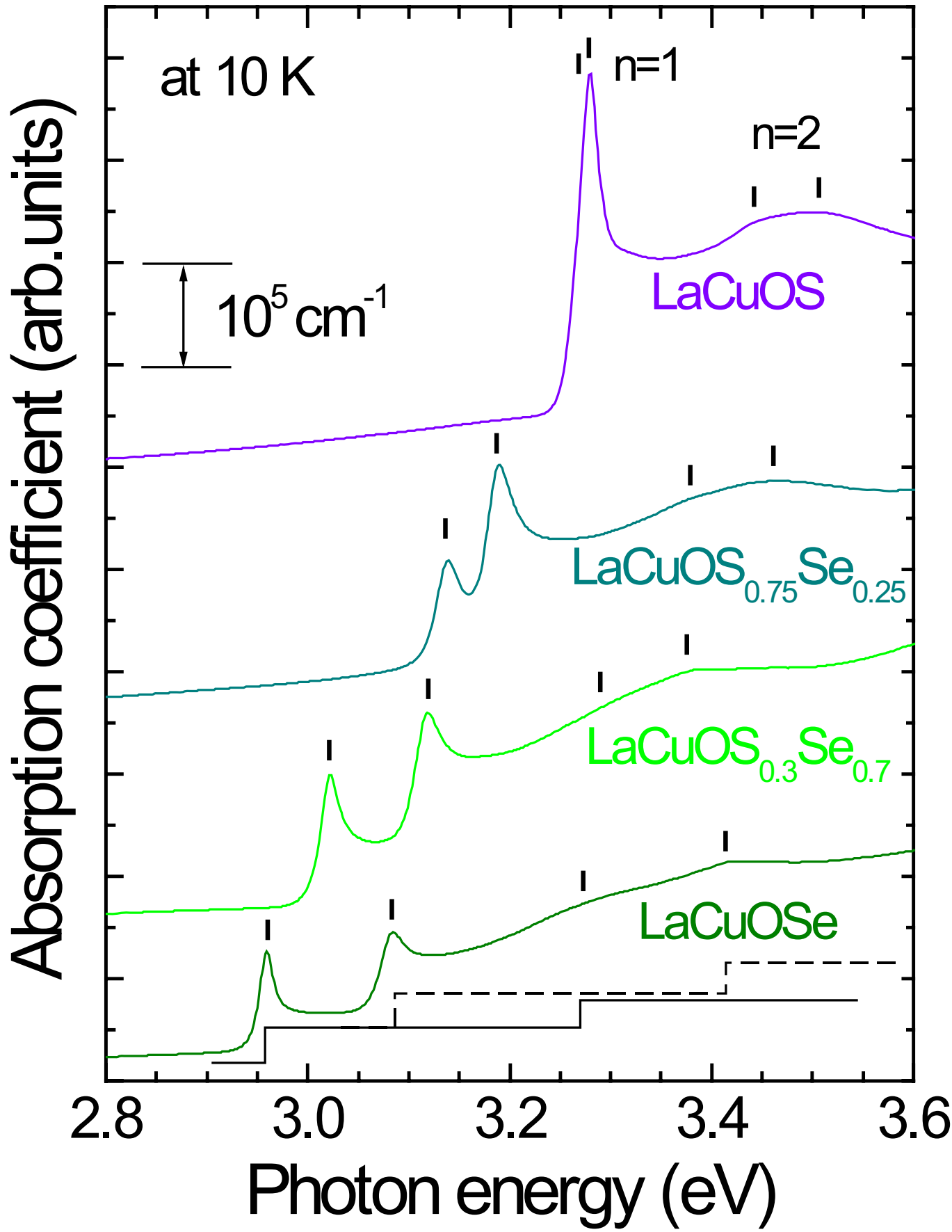
at 10 K
n=1
n=2
10^5 cm^{-1}
LaCuOS
$LaCuOS_{0.75}Se_{0.25}$
$LaCuOS_{0.3}Se_{0.7}$
LaCuOSe
Absorption coefficient (arb.units)
2.8
3.0
3.2
3.4
3.6
Photon energy (eV)

Figure 11

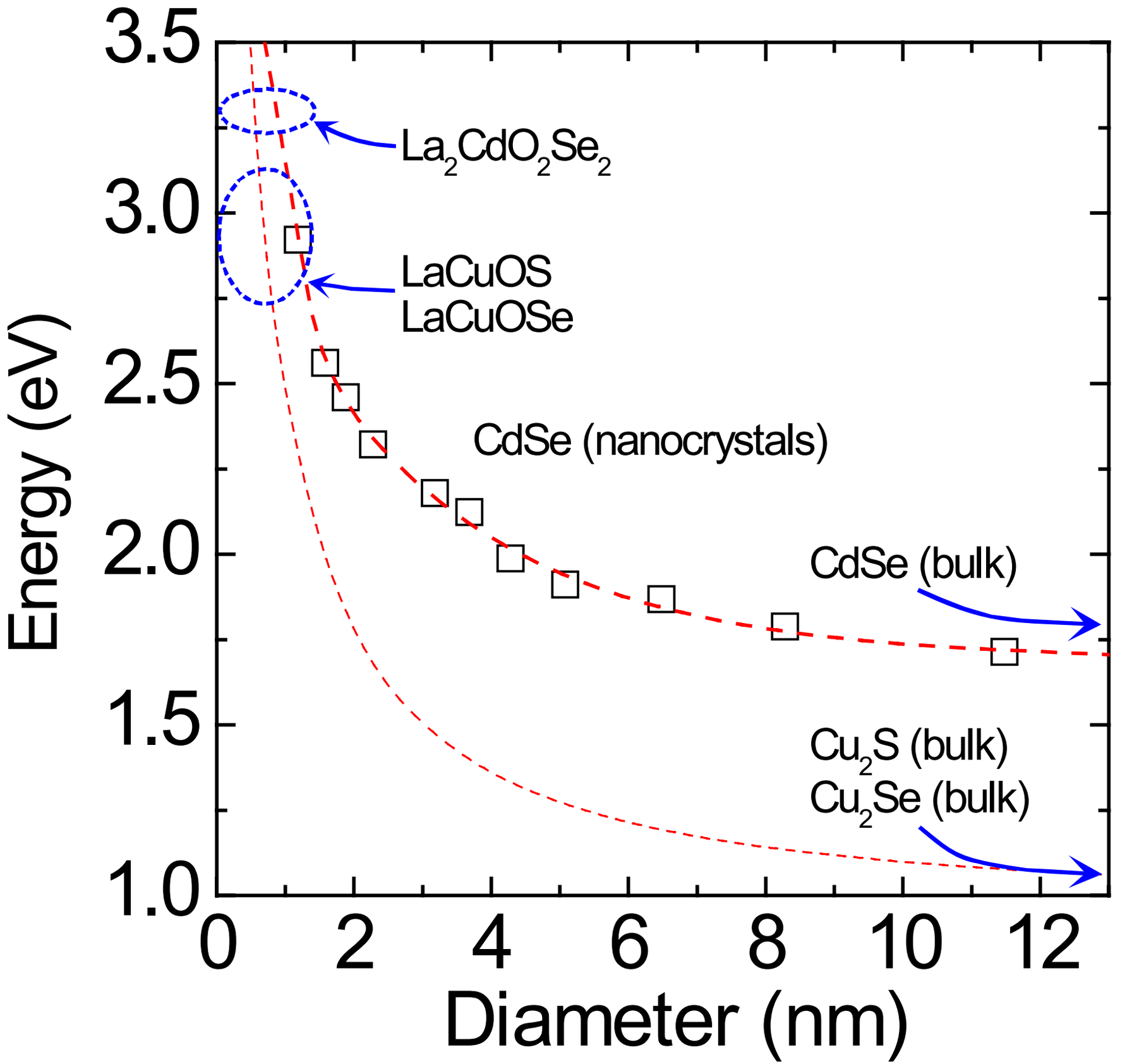
3.5
3.0
2.5
2.0
1.5
1.0
Energy (eV)
0
2
4
6
8
10
12
Diameter (nm)
La2CdO2Se2
LaCuOS
LaCuOSe
CdSe (nanocrystals)
CdSe (bulk)
Cu2S (bulk)
Cu2Se (bulk)